sciendo

Gamma radiation shielding properties of (x)Bi$_2$O$_3$–(0.5 − x)ZnO–0.2B$_2$O$_3$–0.3SiO$_2$ glass system

Bonginkosi Vincent Kheswa ⓘ

Abstract. Lead (Pb)-based materials are very effective in radiation shielding due to their high density of Pb. However, they pose health risks to humans because of the toxicity of lead. As a result, the investigation of radiation shielding properties of various lead-free glass materials has drawn a lot of attention from researchers. In this work, the γ radiation competence of the Bi$_2$O$_3$–ZnO–B$_2$O$_3$–SiO$_2$ glass network was investigated, for the first time in the 0.015–15 MeV energy range, using Phy-X/PSD and XCOM software systems. The results showed that 45Bi$_2$O$_3$–5ZnO–20B$_2$O$_3$–30SiO$_2$ glass sample has the highest linear attenuation coefficient, mass attenuation coefficient, and effective atomic number, and it has the lowest half-value layer, tenth-value layer, and mean-free path. Therefore, 45Bi$_2$O$_3$–5ZnO–20B$_2$O$_3$–30SiO sample is more effective on γ ray shielding than 10Bi$_2$O$_3$–40ZnO–20B$_2$O$_3$–30SiO, 20Bi$_2$O$_3$–30ZnO–20B$_2$O$_3$–30SiO, 30Bi$_2$O$_3$–20ZnO–20B$_2$O$_3$–30SiO, and 40Bi$_2$O$_3$–10ZnO–20B$_2$O$_3$–30SiO samples. The comparison of the results with the literature also revealed that the 45Bi$_2$O$_3$–5ZnO–20B$_2$O$_3$–30SiO glass sample is even more effective than some of Bi$_2$O$_3$-based glass systems, which were recently developed in the literature, by at least a factor of 2.

Keywords: Bismuth-oxide • Glass • Bi$_2$O$_3$–ZnO–B$_2$O$_3$–SiO$_2$ • γ-ray shielding • Heavy metal oxide

Introduction

Gamma (γ) radiation is emitted from an excited nucleus when it de-excites from high energy levels to lower energy levels and loses energy in the form of γ rays. The energy of γ rays is equal to the difference between the energies of the quantum states between which the nucleus is de-exciting. Gamma rays are found in various industries for different applications. For instance, they are used in particle accelerator facilities for γ spectroscopy research and in the sterilization industry for irradiation of surgical instruments and art objects to eliminate microbes such as viruses and bacteria. On the other hand, γ rays have high energies, in the MeV range, and hence they are highly penetrative and damaging to living cells. Thus, they are hazardous to humans who are working with them. However, these radiation hazards can be prevented through effective radiation shielding techniques.

The traditional method of shielding γ rays is by the usage of lead (Pb)-based shielding materials, which have been investigated in many studies [1–4] and proven effective. However, due to the toxicity of Pb, recent studies are investigating alternative solutions. In particular, the possible usage of Pb-free heavy metal oxide (HMO)-based glasses is being studied. This area of research is currently an

B. V. Kheswa
Department of Physics
University of Johannesburg
Johannesburg, 2028, South Africa
E-mail: vincentk@uj.ac.za

area of interest to many researchers around the globe [5–15]. For instance, the study of Ahmad *et al.* [12] investigated the γ ray shielding capacity of x[Bi_2O_3] + (0.5 – x)[ZnO] + 0.2[B_2O_3] + 0.3[Soda Lime Silica] glass, where x = 0.05, 0.10, 0.20, 0.30, 0.40, and 0.45, and showed that it is enhanced by the increase in the concentration of Bi_2O_3. In the same vein, Kurtulus *et al.* [13] investigated the impact of Bi_2O_3 on the γ radiation shielding properties of $10Na_2O$–$6MgO$–$9CaO$–$5Al_2O_3$–$12B_2O_3$–$(100 – x)SiO_2$–xBi_2O_3 (x = 0, 2.5, 5, 7.5, and 10 mol%) glass system and found that the increase in Bi_2O_3 concentration improves the radiation shielding ability of this glass system. Al-Harbi *et al.* also showed that Bi_2O_3 yields better γ radiation shielding capacity than SrO, TeO_2, and PbO in the Li_2O–K_2O–B_2O_3–HMO (HMO = SrO/TeO_2/PbO/Bi_2O_3) glass system [14].

Recently, the study of Mustafa *et al.* [15] manufactured $(x)Bi_2O_3$–$(50 – x)ZnO$–$20B_2O_3$–$30SiO_2$ (where x = 10, 20, 30, 40, and 45 mol%) glass samples and reported on their optical properties. The γ radiation shielding properties of this Bi_2O_3--based glass system have not been investigated in the literature. Even though the study of Mustafa *et al.* [16] reported on the very similar samples such as $(x)Bi_2O_3$–$(1 – x)ZnO$–$0.2B_2O_3$–$0.3(SiO_2)$RHA glass where x = 0.1, 0.2, 0.3, 0.4, and 0.5 and RHA = rice husk ash), it only looked at one γ ray energy which is 0.05459 MeV. Thus, in this work, the γ radiation shielding properties of the $(x)Bi_2O_3$–$(50 – x)ZnO$ –$20B_2O_3$–$30SiO_2$ glasses were studied in detail, in the 0.015 MeV to 15 MeV energy region, and compared with those of other Bi_2O_3-based lead-free glasses. In particular, their linear attenuation coefficient (LAC), mass attenuation coefficient (MAC), half-value layer (HVL), tenth-value (TVL), mean--free path (MFP), and effective atomic number (Z_{eff}) were simulated using the Phy-X/PSD and XCOM software systems for photon energies ranging from 0.015 MeV to 15 MeV. These simulation programs were chosen because they have been extensively used and rigorously tested, in the literature, on various HMO glass materials with Pb and Bi in the mass region, including lead-based glasses. In particular, they have been compared with experimental data and simulations of other materials which were done using Monte-Carlo codes such as MCNP (see Refs. [7, 13, 17] and references therein). Thus, we have confidence on the results from Phy-X/PSD and XCOM.

Computational methods

In radiation shielding applications, the LAC, MAC, HVL, TVL, MFP, and Z_{eff} are very critical quantities. The LAC and MAC describe the probability that photons will interact with a medium. The greater the values of these parameters, the better the material is in shielding γ rays. On the other hand, the HVL and TVL are absorber thicknesses that are required to attenuate photons by 50% and 90%, respectively. Hence, small values of the HVL and TVL represent better radiation shielding ability of a material. Furthermore, the MFP is the average distance between

Table 1. The chemical contents (mol%) of glass samples used in this study [15]

Sample code	Bi_2O_3	ZnO	B_2O_3	SiO_2	Density (g/cm³)
S1	10	40	20	30	4.59
S2	20	30	20	30	4.97
S3	30	20	20	30	5.87
S4	40	10	20	30	6.20
S5	45	5	20	30	6.31

two consecutive interactions of a photon, while Z_{eff} is the effective atomic number of an absorber. Thus, low values of the MFP and high values of Z_{eff} represent better radiation shielding ability of a material.

In this work, the γ rays shielding properties of the B_2O_3–Bi_2O_3–ZnO–SiO_2 glass system were simulated for the samples S1, S2, S3, S4, and S5, of which the chemical contents are shown in Table 1. This was achieved using Phy-X/PSD simulation software [18, 19]. Phy-X/PSD is a recently developed user--friendly software that runs remotely on the Ubuntu operating system. It can calculate radiation shielding parameters for photon energies between 0.001 MeV and 100 GeV. The primary input data required by the software in these calculations are the chemical contents and densities of the samples, which are shown in Table 1 for this work. Using these, it can calculate MAC, HVL, TVL, MFP, and Z_{eff}, of different glass samples, from the corresponding LAC, using the theoretical equations which are discussed in detail below. The XCOM program [20] also requires the samples' densities and chemical contents to compute the corresponding MAC, based on its database. These MACs can be directly converted to LAC, HVL, TVT, MFP, and Z_{eff}, using the equations below.

According to the well-known Beer–Lambert law, the LAC, μ, of a sample is related to the beam intensity and thickness of the absorber as follows:

$$(1) \qquad I_f = I_i \exp(-\mu x)$$

where I_i and I_f are, respectively, the unattenuated and attenuated photon intensities, and *x* is the thickness of the absorber. The LAC can also be computed from the MAC, μ_m, according to Sakar *et al.* [18]:

$$(2) \qquad \mu = \rho\mu_m$$

where ρ is the sample density. The MAC of a composite sample is given by Sakar *et al.* [18]:

$$(3) \qquad \mu_m = \sum_j w_j \left(\frac{\mu}{\rho}\right)_j$$

where $(\mu/\rho)_j$ and w_j are the MAC and weight fraction of a *j*th element in the sample. Using the LAC, the HVL, TVL, and MFP of the sample can be determined as follows [18]:

$$(4) \qquad HVL = \frac{\ln 2}{\mu}$$

$$(5) \qquad TVL = \frac{\ln 10}{\mu}$$

(6)
$$\text{MFP} = \frac{1}{\mu}$$

Furthermore, the effective atomic number is computed from the MACs of the constituents using the expression below [18]:

(7)
$$Z_{\text{eff}} = \frac{\sum_j f_j A_j \left(\dfrac{\mu}{\rho}\right)_j}{\sum_j \dfrac{f_j A_j}{Z_j} \left(\dfrac{\mu}{\rho}\right)_j}$$

where f_j, A_j, and Z_j are, respectively, the mole fraction of each element, atomic weight, and atomic number in the sample.

Results and discussions

This section contains the discussion of the results on the LAC, MAC, HVL, TVL, MFP, and effective atomic number (Z_{eff}), which were obtained using Phy-X/PSD software. The LAC and MAC as a function of γ energy are depicted in Figs. 1 and 2, in the photon energy range of 0.015 MeV to 15 MeV, respectively. Figure 1 shows that the LAC decreases fast with the increase in photon energy at energies <0.1 MeV and suddenly increases at 0.1 MeV and decreases sharply again up to 1 MeV, above which it decreases slowly and remains relatively constant >3 MeV. This fast decrease of the LAC is due to the photoelectric effect of which the contribution to the LAC decreases significantly with an increase in photon energy. The enhancement at 0.1 MeV is due to the K shell electrons which start contributing to the photoelectric effect at 0.1 MeV. This behavior of the LAC as a function of gamma energy is similar to what has been observed in the literature [11, 21]. It is also observed in Fig. 1 that S1 has the lowest LAC, and S5 has the highest LAC. In particular, the LAC ranges from 293.938 cm to 0.169 cm, 380.051 cm to 0.210 cm, 491.990 cm to 0.267 cm, 549.723 cm to 0.295 cm, and 571.187 cm to 0.306 cm for S1, S2, S3, S4, and S5, respectively. Clearly, it has increased significantly with an increase in the Bi$_2$O$_3$ concentra-
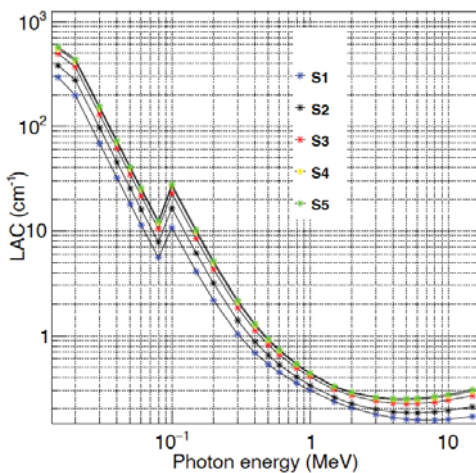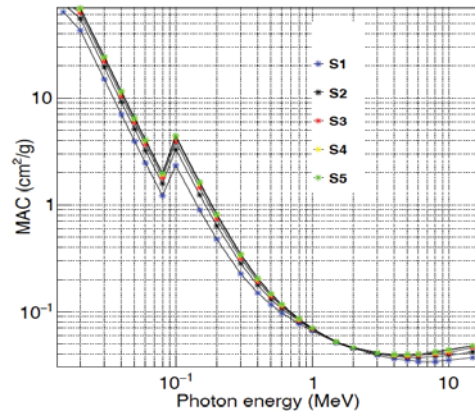

Fig. 2. Mass attenuation coefficient of glass samples S1, S2, S3, S4, and S5.

tion. This trend is also consistent with the literature [17]. Furthermore, Fig. 2 shows that the behavior of the MAC as a function of γ ray energy is similar to the one of the LAC, except for energies between 1 MeV and 3 MeV where the MAC of all samples are comparable.

Furthermore, the Phy-X/PSD software calculations were validated using XCOM software. In particular, we compared the LAC obtained using Phy-X/PSD with the LAC from XCOM calculations, in the similar fashion that was recently used in the literature [22]. The comparison of the LAC from the two software systems is shown in Fig. 3. There is
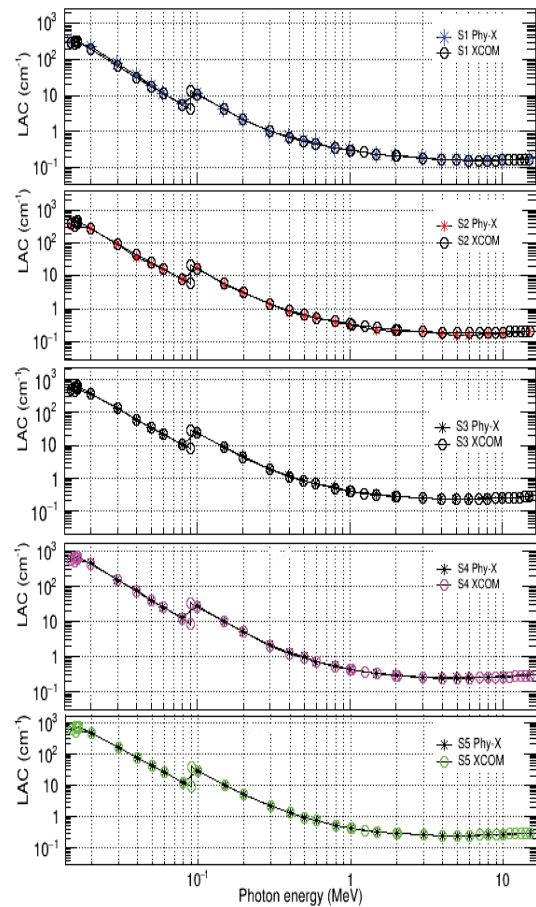

Fig. 3. Comparison of LAC from Phy-X/PSD and XCOM for S1, S2, S3, S4, and S5.
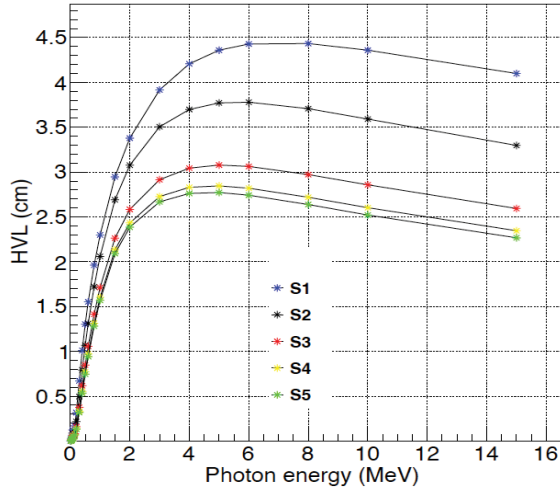

Fig. 1. Linear attenuation coefficient of glass samples S1, S2, S3, S4, and S5.

Fig. 4. Half-value layer of glass samples S1, S2, S3, S4, and S5.

Fig. 5. Tenth-value layer of glass samples S1, S2, S3, S4, and S5.

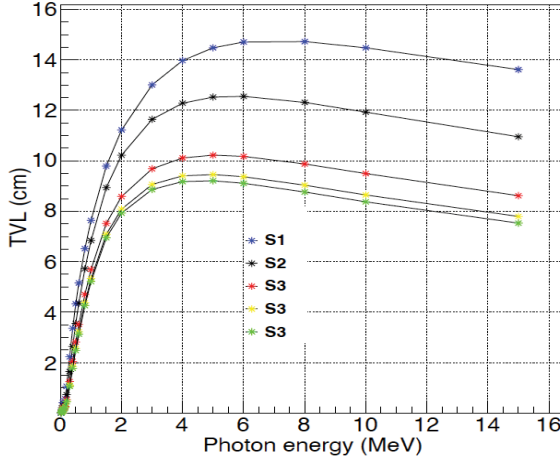**Fig. 6.** Mean-free path of glass samples S1, S2, S3, S4, and S5.

Fig. 7. Effective atomic number of glass samples S1, S2, S3, S4, and S5.

an excellent agreement between the two simulation software systems for our five glass samples, hence providing confidence on the results that were calculated using Phy-X/PSD software. There was no need to further compare the rest of the radiation shielding quantities because they are derived from the LAC, on which we already had confidence.

The HVL and TVL are, respectively, depicted in Figs. 4 and 5, as a function of γ ray energy, for all samples that were studied in this work. It is clear that glass S1 has the highest HVL and TVL, while glass S5 has the lowest HVL and TVL. In particular, the HVL is in the range of 0.002–4.433 cm, 0.002–3.779 cm, 0.001–3.078 cm, 0.001–2.846 cm, and 0.001–2.772 cm for S1, S2, S3, S4, and S5, respectively. On the other hand, the TVL for S1, S2, S3, S4, and S5 ranges from 0.008 cm to 14.726 cm, 0.006 cm to 12.554 cm, 0.005 cm to 10.223 cm, 0.004 cm to 9.454 cm, and 0.004 cm to 9.207 cm, respectively. Clearly, the HVL and TVL of the Bi_2O_3–ZnO–B_2O_3–SiO_2 glass system decrease with the increase in the content of Bi_2O_3. It is also seen that the HVL and TVL increase sharply with the increase in γ ray energy, up to 5 MeV after which they remain approximately constant. The trends observed in the HVL and TVL of the present work have been reported in other studies [23, 24].
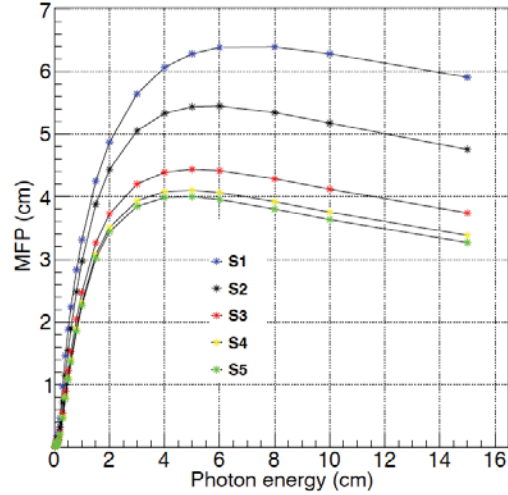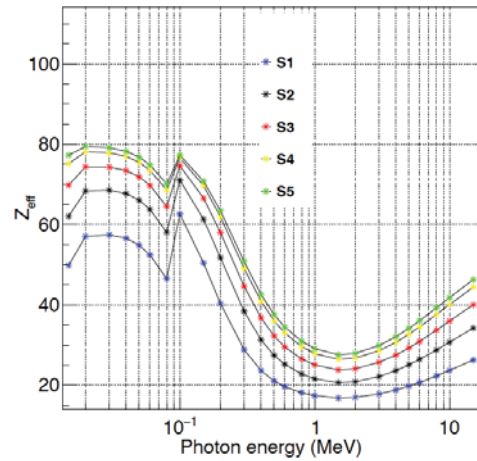
Figure 6 shows MFPs of the samples S1, S2, S3, S4, and S5 in the 0.015 MeV to 15 MeV photon energy range. It is observed that glass S1 has the highest MFP, while glass S5 has the lowest MFP. In fact, the MFP of S1, S2, S3, S4, and S5 is in the range of 0.003–6.395 cm, 0.003–5.452 cm, 0.002–4.440 cm, 0.002–4.106 cm, and 0.002–3.999 cm, respectively. It is also clear that the MFP increases fast with the increase in the photon energy for energies <5 MeV and remains relatively constant at energies >5 MeV. This relationship of the MFP with energy is consistent with the distribution of the LAC shown in Fig. 1. It is also consistent with the literature [25, 26].

In Fig. 7, the effective atomic number (Z_{eff}) of the Bi_2O_3–ZnO–B_2O_3–SiO_2 glass system is shown, as a function of photon energy in the range of 0.015–15 MeV. This quantity decreases with the increase in photon energies <0.1 MeV, which is enhanced and after which it continues decreasing sharply up to the photon energy of 1 MeV. It remains relatively constant between 1 MeV and 3 MeV and increases slowly with the increase in energies >3 MeV. The distribution of Z_{eff} that is similar to the one observed in this study has been recently reported in the literature [27]. It is also clear that S1, which has the lowest Bi_2O_3 content, and S5, which has the high-
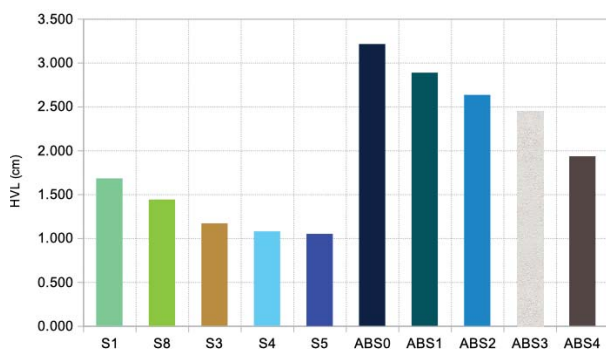
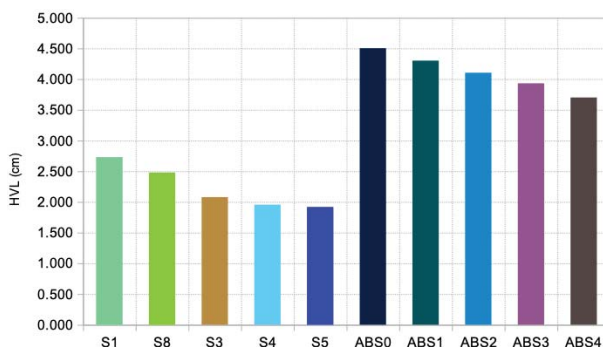**Fig. 8.** Comparison of the half-value layer with literature at 0.662 MeV.

Fig. 9. Comparison of the half-value layer with literature at 1.332 MeV.

est Bi_2O_3 content, have the lowest and highest Z_{eff}, respectively. It ranges from 62.68 to 16.82 for S1, 71.10 to 20.66 for S2, 74.66 to 23.81 for S3, 78.10 to 26.44 for S4, and 79.46 to 27.60 for S5.

Furthermore, the radiation shielding abilities of the glass samples S1, S2, S3, S4, and S5 were compared with those of other Bi_2O_3-based glasses that have been investigated in the literature. In particular, the HVL of all samples studied in this work was compared with the HVL of ABS0 ($10Na_2O-6MgO-9CaO-5Al_2O_3-12B_2O_3-58SiO_2$), ABS1 ($10Na_2O-6MgO-9CaO-5Al_2O_3-12B_2O_3-55.5SiO_2-2.5Bi_2O_3$), ABS2 ($10Na_2O-6MgO-9CaO-5Al_2O_3-12B_2O_3-53SiO_2-5Bi_2O_3$), ABS3 ($10Na_2O-6MgO-9CaO-5Al_2O_3-12B_2O_3-50.5SiO_2-7.5Bi_2O_3$), and ABS4 ($10Na_2O-6MgO-9CaO-5Al_2O_3-12B_2O_3-48SiO_2-10Bi_2O_3$) from Ref. [13]. They were also compared with Bi1 ($5Bi_2O_3+45ZnO+20B_2O_3+30SLS$), Bi2 ($10Bi_2O_3+40ZnO+20B_2O_3+30SLS$), Bi3 ($20Bi_2O_3+30ZnO+20B_2O_3+30SLS$), Bi4 ($30Bi_2O_3+20ZnO+20B_2O_3+30SLS$), Bi5 ($40Bi_2O_3+10ZnO+20B_2O_3+30SLS$), and Bi6 ($45Bi_2O_3+5ZnO+20B_2O_3+30SLS$) from Ref. [12]. Figures 8 and 9 show that the samples S1, S2, S3, S4, and S5 have smaller HVL than ABS0, ABS1, ABS2, ABS3, and ABS4 at photon energies of 0.662 MeV and 1.332 MeV. Sample S5 has the lowest, and it is lower than that of ABS4, which is the lowest in Ref. [13], by almost a factor of 2.

Figure 10 shows the comparison of HVL of the glass materials of this study and Bi1, Bi2, Bi3, Bi4, Bi5, and Bi6 at 0.662 MeV. This comparison also shows that S1, S2, S3, S4, and S5 have lower
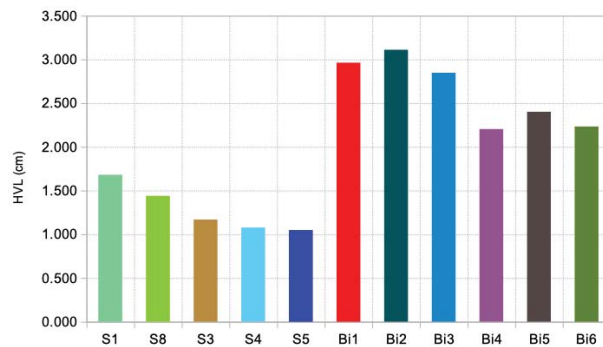

Fig. 10. Second comparison of the half-value layer with literature at 0.662 MeV.

HVL than Bi1, Bi2, Bi3, Bi4, Bi5, and Bi6, and S5 remains the lowest. It is also observed that the HVL of sample S5 is less than the HVL of Bi4, which is the lowest in Ref. [12], by more than a factor of 2.

Conclusion

The radiation shielding properties of $(x)Bi_2O_3-(50-x)ZnO-20B_2O_3-30SiO_2$ (where x = 10, 20, 30, 40, and 45 mol%) glass system were investigated. The LAC, MAC, HVL, TVL, MFP, and Z_{eff} of this glass network were computed using Phy-X/PSD simulation software, which was validated using XCOM software. The $45Bi_2O_3-5ZnO-20B_2O_3-30SiO_2$ sample has the highest LAC, MAC, and Z_{eff} and the lowest HVL, TVL, and MFP. In particular, its LAC, MAC, and Z_{eff} are in the ranges of 571.187–0.306 cm, 90.521–0.040 cm, and 79.46–27.60 cm, respectively, while the HVL, TVL, and MFP range from 0.001 cm to 2.772 cm, 0.004 cm to 9.207 cm, and 0.002 cm to 3.999 cm, respectively. Thus, the $45Bi_2O_3-5ZnO-20B_2O_3-30SiO_2$ glass is the most effective radiation shielding material in the $(x)Bi_2O_3-(50-x)ZnO-20B_2O_3-30SiO_2$ (where x = 10, 20, 30, 40, and 45 mol%) glass system.

The results of this work were also compared with those of the literature. This comparison revealed that the $45Bi_2O_3-5ZnO-20B_2O_3-30SiO_2$ glass sample, which was studied in this work, has lower HVL than $10Na_2O-6MgO-9CaO-5Al_2O_3-12B_2O_3-(58-x)SiO_2-(x)Bi_2O_3$ (where x = 0, 2.5, 5, 7.5, and 10 mol%) and $(x)Bi_2O_3+(50-x)ZnO+20B_2O_3+30SLS$ (where x = 0, 5, 10, 20, 30, 40 and 45 mol%) glass systems, by at least a factor of 2. Therefore, the $45Bi_2O_3-5ZnO-20B_2O_3-30SiO_2$ glass is more effective than some of the Bi_2O_3-based glasses by at least a factor of 2 that have been recently studied in the literature.

ORCID

B. V. Kheswa http://orcid.org/0000-0003-3044-094X

References

1. Kirdsiri, K., Kaewkhao, J., Chanthima, N., & Limsuwan, P. (2011). Comparative study of silicate glasses containing Bi_2O_3, PbO and BaO: Radiation shielding and optical properties. *Ann. Nucl. Energy*, *38*(6), 1438–1441. https://doi.org/10.1016/j.anucene.2011.01.031.

2. Kumar, A. (2017). Gamma ray shielding properties of $PbO-Li_2O-B_2O_3$ glasses. *Radiat. Phys. Chem.*, *136*, 50–53. https://doi.org/10.1016/j.radphyschem.2017.03.02.

3. Kaur, S., & Singh, K. (2014). Investigation of lead borate glasses doped with aluminium oxide as gamma ray shielding materials. *Ann. Nucl. Energy*, *63*, 350–354. https://doi.org/10.1016/j.anucene.2013.08.012.

4. Roy, S. C., & Sandison, G. A. (2000) Shielding for neutron scattered dose to the fetus in patients treated with 18 MV x-ray beams. *Med. Phys.*, *27*, 1800. https://doi.org/10.1118/1.1287438.

5. Sayyed, M., Çelikbilek Ersundu, M., Ersundu, A. E., Lakshminarayana, G., & Kostka, P. (2018). Investigation of radiation shielding properties for MeO-$PbCl_2$-TeO_2 (MeO = Bi_2O_3, MoO_3, Sb_2O_3, WO_3, ZnO) glasses. *Radiat. Phys. Chem.*, *144*, 419–425. http://dx.doi.org/10.1016/j.radphyschem.2017.10.005.

6. Akkurt, I., Malidarre, R., & Kavas, T. (2021). Monte Carlo simulation of radiation shielding properties of the glass system containing Bi_2O_3. *Eur. Phys. J. Plus*, *136*, 264. https://doi.org/10.1140/epjp/s13360-021-01260-y.

7. Kaewkhao, J., Pokaipisit, A., & Limsuwan, P. (2010). Study on borate glass system containing with Bi_2O_3 and BaO for gamma-rays shielding materials: Comparison with PbO. *J. Nucl. Mater.*, *399*(1), 38–40. DOI: 10.1016/j.jnucmat.2009.12.020.

8. Sayyed, M., Elbashir, B., Tekin, H., Altunsoy, E., & Gaikwad, D. (2018). Radiation shielding properties of pentaternary borate glasses using MCNPX code. *J. Phys. Chem. Solids*, *121*, 17–21. https://doi.org/10.1016/j.jpcs.2018.05.009.

9. Sopapan, P., Laopaiboon, J., Jaiboon, O., Yenchai, C., & Laopaiboon, R. (2020). Feasibility study of recycled CRT glass on elastic and radiation shielding properties used as x-ray and gamma-ray shielding materials. *Prog. Nucl. Energy*, *119*, 103149. https://doi.org/10.1016/j.pnucene.2019.103149.

10. Waly, E. S. A., Fusco, M. A., & Bourham, M. A. (2016). Gamma-ray mass attenuation coefficient and half value layer factor of some oxide glass shielding materials. *Ann. Nucl. Energy*, *96*, 26–30. https://doi.org/10.1016/j.anucene.2016.05.028.

11. ALMisned, G., Elshami, W., Issa, S., Susoy, G., Zakaly, H., Algethami, M., Rammah, Y., Ene, A., Al-Ghamdi, S., Ibraheem, A. A., & Tekin, H. O. (2021). Enhancement of gamma-ray shielding properties in cobalt-doped heavy metal borate glasses: The role of lanthanum oxide reinforcement. *Materials*, *14*, 7703. https://doi.org/10.3390/ma14247703.

12. Ahmad, N. S., Mustafa, I. S., Mansor, I., Malik, M. F. I. A., Razali, N. A. N., & Nordin, S. (2018). Gamma ray shielding characteristic of BiZnBo-SLS and PbZnBo-SLS glass. *Mater. Res. Express*, *5*(5), 055203. https://doi.org/10.1088/2053-1591/aac1d1.

13. Kurtulus, R., Kavas, T., Akkurt, I., Gunoglu, K., Tekin, H. O., & Kurtulus, C. (2021). A comprehensive study on novel alumino-borosilicate glass reinforced with Bi_2O_3 for radiation shielding applications: synthesis, spectrometer, XCOM, and MCNP-X works. *J. Mater. Sci.-Mater. Electron.*, *32*, 13882–13896. https://doi.org/10.1007/s10854-021-05964-w.

14. Al-Harbi, F. F., Prabhu, N. S., Sayyed, M. I., Almuqrin, A. H., Kumar, A., & Kamath, S. D. (2021). Evaluation of structural and gamma ray shielding competence of $Li_2O-K_2O-B_2O_3$-HMO (HMO = $SrO/TeO_2/PbO/Bi_2O_3$) glass system. *Opt. (Stuttg)*, *248*, 168074. https://doi.org/10.1016/j.ijleo.2021.168074.

15. Mustafa, I. S., Razali, N. A. N., Azman, N. Z. N., Yahaya, N. Z., Zaini, M. Z. M., Rusli, N. L., Nizamani, M. B., & Kamari, H. M. (2017). Comprehensive study of electronic polarizability and band gap of B_2O_3–Bi_2O_3–ZnO–SiO_2 glass network. *J. Adv. Dielectr.*, *7*(5), 1750031. https://doi.org/10.1142/S2010135X1750031X.

16. Mustafa, I. S., Razali, N. A. N., Ibrahim, A. R., Yahaya, N. Z., & Kamari, H. M. (2015). From rice husk to transparent radiation protection material. *Jurnal Intelek*, *9*(2), 1–6.

17. Akkurt, I., Malidarre, R., & Kavas, T. (2021). Monte Carlo simulation of radiation shielding properties of the glass system containing Bi_2O_3. *Eur. Phys. J. Plus*, *136*, 264. https://doi.org/10.1140/epjp/s13360-021-01260-y.

18. Sakar, E., Ozpolat, O., Alım, B., Sayyed, M., & Kurudirek, M. (2020). Phy-X/PSD: Development of a user friendly online software for calculation of parameters relevant to radiation shielding and dosimetry. *Phys. Chem.*, *166*, 108496. https://doi.org/10.1016/j.radphyschem.2019.108496.

19. Phy-X/PSD: Photon Shielding and Dosimetry. https://phy-x.net/PSD.

20. XCOM [database]. National Institute of Standards and Technology. https://physics.nist.gov/PhysRefData/Xcom/html/xcom1.html.

21. Sarihan, M. (2020). Simulation of gamma-ray shielding properties for materials of medical interest. *Open Chem.*, *20*, 81–87. https://doi.org/10.1515/chem-2021-0118.

22. Kheswa, B. V. (2023). X-ray shielding properties of bismuth-borate glass doped with rare-earth ions. *Open Chem.*, *21*, 20220345. https://doi.org/10.1515/chem-2022-0345.

23. Kaur, P., Singh, K. J., Thakur, S., & Kurudirek, M. (2020). Investigation of a competent non-toxic Bi_2O_3-Li_2O-CeO_2-MoO_3-B_2O_3 glass system for nuclear radiation security applications. *J. Non. Cryst. Solids*, *545*, 120235. https://doi.org/10.1016/j.jnoncrysol.2020.120235.

24. Sayyed, M. I., Kurtulus, R., Balderas, C. V., Kavas, T., & Almuqrin, A. H. (2021). Xray shielding behavior of $TeO_2Li_2OGeO_2ZnOBi_2O_3$ glass system using EPICS2017 library and PhyX software. *Appl. Phys. A*, *127*, 757. https://doi.org/10.1007/s00339-021-04893-z.

25. Kavaz, E., Agawany, F. E., Tekin, H., Perisanoglu, U., & Rammah, Y. S. (2020). Nuclear radiation shielding using barium borosilicate glass ceramics. *J. Phys. Chem. Solids*, *142*, 109437. https://doi.org/10.1016/j.jpcs.2020.109437.

26. Mhareb, M. H. A. (2020). Physical, optical and shielding features of Li_2O–B_2O_3–MgO–Er_2O_3 glasses

co-doped of Sm$_2$O$_3$. *Appl. Phys. A*, *126*, 71. https://doi.org/10.1007/s00339-019-3262-9.

27. Tekin, H. O., ALMisned, G., Zakaly, H. M. H., Zamil, A., Khoucheich, D., Bilal, G., Al-Sammarraie, L., Issa, S. A. M., Al-Buriahi, M. S., & Ene, A. (2022).

Gamma, neutron, and heavy charged ion shielding properties of Er^{3+}-doped and Sm^{3+}-doped zinc borate glasses. *Open Chem*., *20*, 130–145. https://doi.org/10.1515/chem-2022-0128.